Hindawi
International Journal of Antennas and Propagation
Volume 2020, Article ID 3268729, 12 pages
https://doi.org/10.1155/2020/3268729

*Research Article*

# A Triband Patch Antenna with Monopole-like and Patch-like Radiation Patterns for Multifunctional Wireless Systems

**Hai-Na Song**,[1] **Zhao-Hui Chen**,[2] **and Jian-Feng Li**[3]

[1]*School of Electronic and Information Engineering, South China University of Technology, Guangzhou, Guangdong 510640, China*
[2]*Guangzhou HaiGe Communications Group Incorporated Company, Guangzhou, Guangdong 510663, China*
[3]*School of Physics & Optoelectronic Engineering, Guangdong University of Technology, Guangzhou, Guangdong 510600, China*

Correspondence should be addressed to Hai-Na Song; 47085509@qq.com

Received 15 January 2020; Revised 17 April 2020; Accepted 8 May 2020; Published 11 June 2020

Academic Editor: Hervé Aubert



A triband patch antenna with monopole-like and patch-like radiation patterns for multifunctional wireless systems is proposed. The antenna consists of a single square radiation patch with an annular slot, a ground plane, and a top-loaded metal sheet. The top-loaded metal sheet is shorted to the ground plane for producing a zeroth-order resonant (ZOR) mode, which has an omnidirectional radiation pattern at the lowest operation band, and its performance is robust to the location of the probe feed. With the annular slot and the off-center probe feed, a dual-resonant $TM_{01}$ mode is excited, yielding unidirectional radiation patterns for the two upper operation bands. The ZOR and the dual-resonant $TM_{01}$ modes can be independently controlled, and a triband antenna prototype with a square patch of 24 mm is fabricated and tested. The first bandwidth is 2.5–2.7 GHz with omnidirectional radiation pattern, the second and the third bandwidths with unidirectional radiation are 3.3–3.9 GHz and 4.8–6.1 GHz, and the realized gains over the three bands are about 2.6, 6.5, and 7.5 dBi, respectively.

## 1. Introduction

With merits of 360° full coverage, low profile, low cost, and easy fabrication, monopolar patch antennas are widely used in portable devices, such as the mobile phone, laptop, and GPS. Center-fed circular patch antennas can excite $TM_{0m}$ modes with omnidirectional radiation patterns in the azimuth plane [1], but suffering narrow bandwidth. Many techniques have been proposed to solve the problem, including disk-loaded [2] and loaded annular ring [3], but the first nonzero mode of these antenna is $TM_{02}$ (1.0 $\lambda$) rather than the eigenmode $TM_{01}$ mode (0.5 $\lambda$), resulting in large antenna sizes. Great efforts have been devoted to the study of $TM_{01}$ mode, the most common method is center-fed circular patch shorted with via holes [4, 5], and monopolar patch antennas with $TM_{01}$ mode were presented [6]. By utilizing shorting vias, annular ring, and stacked patch, monopolar radiation patterns were obtained over a broadband [7] or two operation bands [8].

Moreover, antennas with monopole-like and patch-like radiation patterns over different bands are desired by multifunctional wireless systems, such as vehicular communications. WMAN (Wireless Metropolitan Area Network) requires omnidirectional signal coverage for vehicular communication system accessing to Internet, and car-to-car communication needs unidirectional signal coverage for safe driving control in vehicular communication systems. To realize the dual-sense radiation patterns, artificial magnetic conductor and shorted vias were employed [9], and a small patch was stacked on a larger patch with vias [10].

Most of dual-sense radiation pattern antennas are circular shaped and center-fed. But triangular, rectangular, and square antennas are also needed in practical applications. Monopolar patch antennas in equilateral triangular shape

[11] and in square-ring shape [12] were presented, while a conical-pattern antenna consisting of four symmetrical square radiating slots and artificial magnetic conductors was studied [13]. Four monopoles shorted to the ground and one square patch loaded with a slot were utilized by the antenna to obtain dual-band and dual-sense radiation patterns [14]. However, the reported antennas suffer from complicated structure and large size.

Resonant frequency of zeroth-order resonant (ZOR) antenna depends on the antenna reactance instead of physical size [15], and that is useful to reduce antenna size. Taking advantage of the mushroom structure, omnidirectional ZOR antennas were proposed [16, 17], and a mushroom patch was inserted in a rectangular patch to generate the ZOR and $TM_{010}$ modes at the same frequency [18]. Utilizing a top-loaded small metal strip, a dual-band circular patch antenna with omnidirectional ZOR mode for the lower band and unidirectional $TM_{01}$ mode for the upper band was studied in [19].

In this paper, a compact triband square patch antenna with monopole-like and patch-like patterns is presented. Compared with the circular patch antenna [19], the proposed square patch antenna has a more compact size and better impedance matching bands to covering more communication bandwidth, so the proposed square patch antenna is more suitable to apply in multifunctional wireless systems. For the proposed square patch antenna, the method for the square radiation patch to excite monopole-like ZOR mode is introducing a rectangular metal sheet, and its performance is robust to the probe feed position. By etching a small annular slot into the square radiation patch, its original $TM_{01}$ mode is split into two $TM_{01}$ modes with controllable resonant frequencies, and they work at the two upper operation bands with unidirectional radiation pattern. Based on the equivalent circuit as well as the distributions of electric field and current, the principles of the antenna are discussed. These concepts are then verified by a triband antenna prototype; it exhibits omnidirectional radiation in 2.5–2.7 GHz and unidirectional radiations in both 3.3–3.9 GHz and 4.8–6.1 GHz. The radiation efficiencies are larger than 77%, 84%, and 86% for the three operation bands, respectively.

## 2. Antenna Design

Figure 1 illustrates the configuration of the proposed antenna; the antenna consists of a square patch with a small annular slot, a ground plane, and a rectangular metal sheet. With an air gap of size $H$ between them, FR4 substrates 1 and 2 have relative permittivity of 4.4, a dielectric loss tangent of 0.002, and a thickness of $H_s = 1.6$ mm. The square ground plane with side length of $L_g$ is printed on the bottom layer of FR4 substrate 1. The square radiation patch with side length of $L_p$ is printed on the bottom layer of FR4 substrate 2 and is fed by an off-center coaxial probe. $F_y$ is the offset distance of the probe feed from the center of the square radiation patch along the $y$-axis. Taking the probe feed as center, a small annular slot with an outer radius $r_1$ and an inner radius $r_2$ is etched in the square radiation patch for producing a dual-resonant $TM_{01}$ mode with unidirectional radiation pattern.

A rectangular metal sheet printed on the top layer of FR4 substrate 2 is shorted to the ground plane through two conductive vias to excite a monopole-like ZOR mode working at the lowest operation band. The dimension of the rectangular metal sheet is $M_l \times M_w$, and the two conductive vias are arranged symmetrically with a distance of $V_d$. There are two clearance circles etched on the radiation patch and are placed around the two conductive vias, respectively, and the radiation patch and the conductive vias are separated.

## 3. Analysis of Working Mechanism

In our design, numerical analysis of the antenna is conducted in the commercial electromagnetic software HFSS in Version 2018, which solves the electric field and magnetic field by using finite element method (FEM). HFSS adopts adaptive mesh generation technology; the solution type and the convergence error are chosen as Driven Modal and 0.01, respectively, in the simulation of the proposed design.

*3.1. Generation of the Dual-Resonant TM01 Mode.* To reveal the operating mechanism of the proposed antenna, a square patch antenna named Design 1 is first investigated. Design 1 has the same dimensions of the proposed antenna shown in Figure 1 but without the metal sheet and the two conductive vias. The resonant frequency $f_0$ of $TM_{01}$ mode is decided by [20, 21]

$$f_0 = \frac{c}{2L_p\sqrt{\varepsilon_{eq}}}, \quad \varepsilon_{eq} = \frac{\varepsilon_{re}(H + H_s)}{H\varepsilon_{re} + H_s}, \tag{1}$$

where $c$ is the velocity of electromagnetic waves in the free space, $\varepsilon_{eq}$ denotes the equivalent permittivity of the substrate with an air gap, $\varepsilon_{re} = 4.4$ is relative permittivity of the substrate, and $H_s = 1.6$ mm and $H = 4$ mm represent the thickness of the substrate and the air between the two substrates. Based on (1), the value of $f_0$ is 4.8 GHz when the square radiation patch side length $L_p = 24$ mm, and that is agreed well with the simulated result for the case of $F_y = 0$ mm, as shown in Figure 2. Coupling existing in the annular slot can split the original $TM_{01}$ mode (at about 4.8 GHz) into two $TM_{01}$ modes. But at the central area of the square radiation patch, the input impedance of the antenna is high due to the strong electric field and the weak magnetic field. Therefore, the impedance matching is poor when $F_y = 0$ mm, and only one $TM_{01}$ mode appears.

A larger $F_y$ means a larger distance between the probe feed and the center of the square patch. With the probe feed moving away from the center, the balance between the electric and magnetic fields can be enhanced to improve the impedance matching gradually, and $TM_{01}$ mode at about $f_0 = 4.8$ GHz is splitted into two $TM_{01}$ modes. Therefore, a dual-resonant $TM_{01}$ mode with controllable resonant frequencies of $f_1$ and $f_2$ is produced, due to the capacitance existing in the annular slot. When the annular slot is close to the central part of the square patch, where antenna input impedance is high, the effect of the annular slot on the

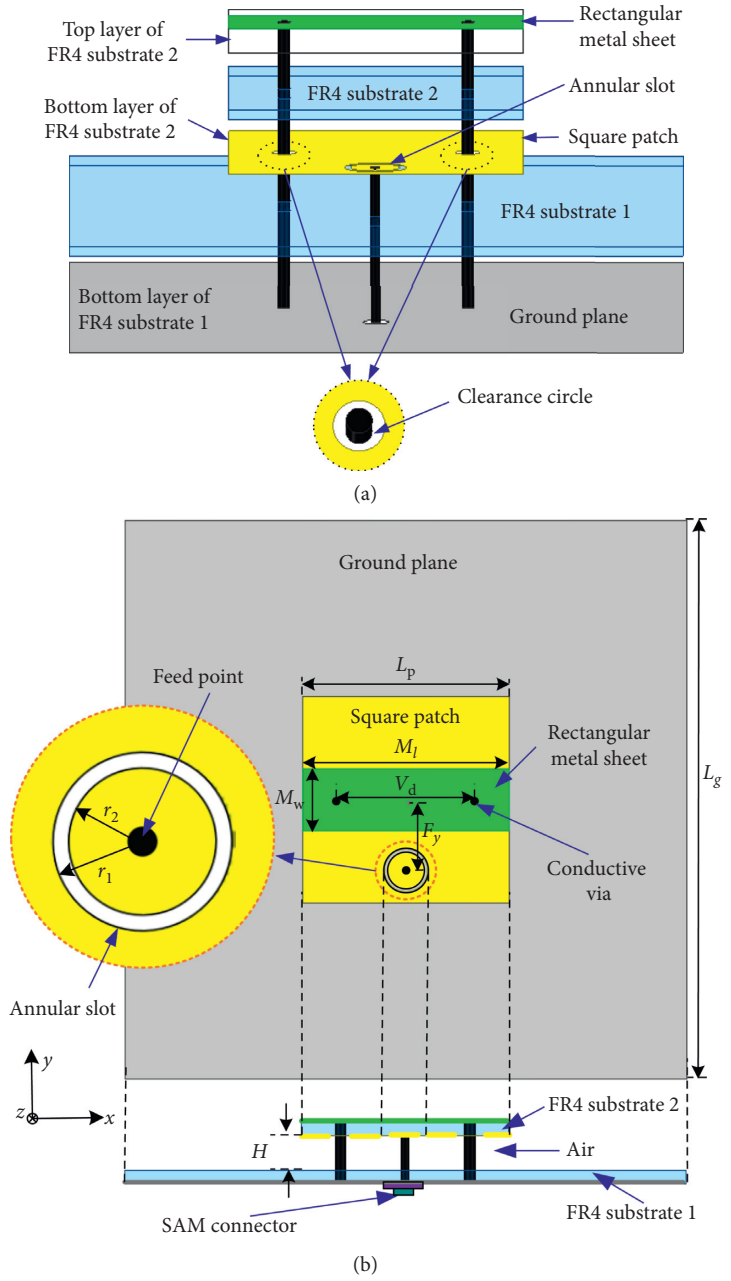


Figure 1: Configuration of the proposed antenna: (a) exploded view; (b) top view and size view. $L_g = 80$ mm, $L_P = 24$ mm, $F_y = 8$ mm, $M_l = 24$ mm, $M_w = 7.2$ mm, $V_d = 15$ mm, $H = 4$ mm, $r_1 = 2.5$ mm, and $r_2 = 2$ mm.

resonant modes will become weak. In other words, with a larger $F_y$, the annular slot has a stronger capacity of splitting the original $TM_{01}$ mode into two $TM_{01}$ modes, so the ratio of $f_1/f_2$ becomes larger, as shown in Figure 2.

Keeping $r_2 = 2.0$ mm, a smaller $r_1$ represents a smaller annular slot width $(r_1 - r_2)$, leading to a stronger coupling of the annular slot, thereby both $f_1$ and $f_2$ shift towards the lower frequencies, as shown in Figure 3. Observing from Figures 2 and 3, we can find that the trends of $f_1$ and $f_2$ are the same with varying $r_1$ but are opposite when $F_y$ is changed, so $f_1$ and $f_2$ can be effectively controlled by tuning $r_1$ and $F_y$, and $r_1$ and $F_y$ are chosen as 3.0 and 8.0 mm for the desired operation bands in the paper.

The current distributions and the simulated 3D radiation patterns of Design 1 at $f_2 = 3.75$ GHz and $f_1 = 5.35$ GHz are shown in Figures 4 and 5, respectively. The off-centered feed can modify the current distribution of the square patch, so the currents have the same direction in general and only one maximum, as shown in Figure 4. That suggests that the two resonant modes of Design 1 at 3.75 and 5.35 GHz are $TM_{01}$ mode, based on the cavity model of patch antenna [22]. For the two $TM_{01}$ modes, the only one theoretical maximum of

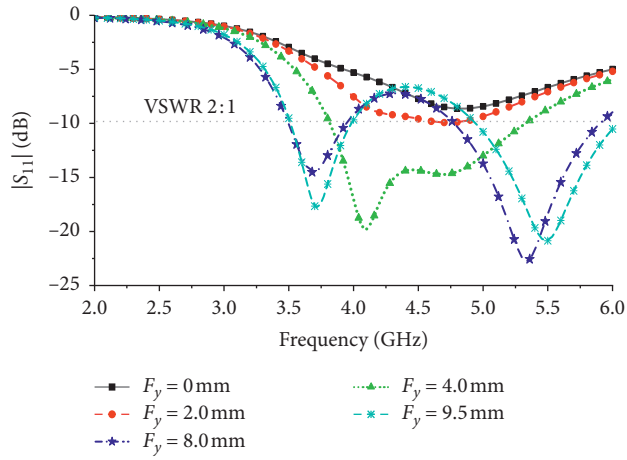


FIGURE 2: Variation of $|S_{11}|$ for Design 1 with respect to $F_y$.

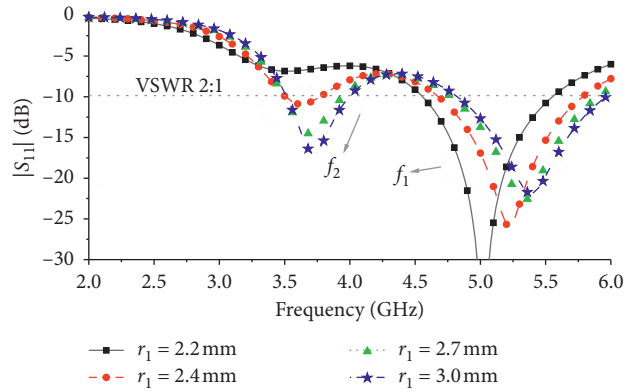


FIGURE 3: Variation of $|S_{11}|$ for Design 1 with respect to $r_1$.

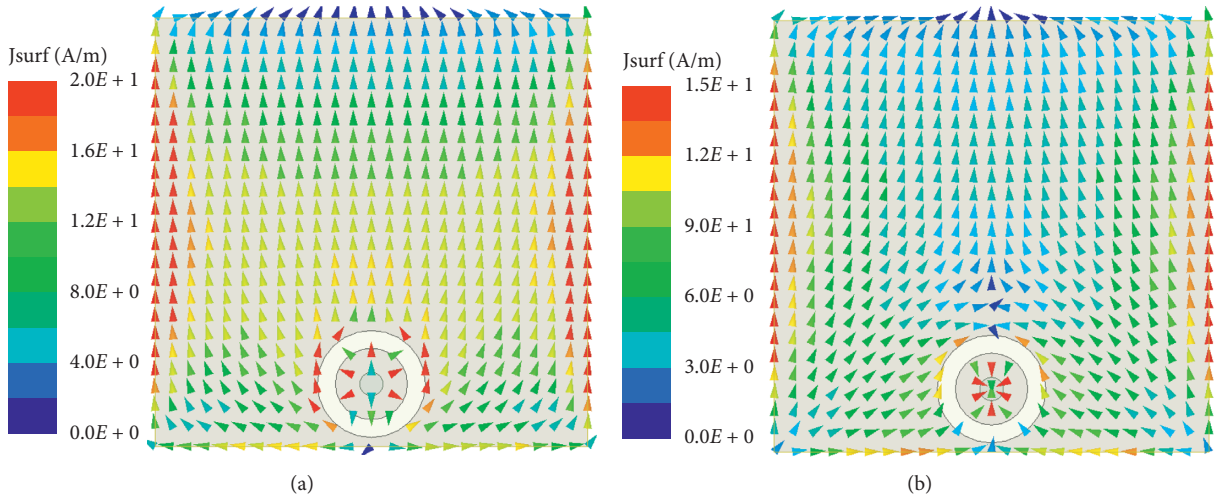


FIGURE 4: Current distributions on the radiation square patch of Design 1: (a) $f_2 = 3.75$ GHz and (b) $f_1 = 5.35$ GHz.

radiation at the broadside direction is obtained in some degree, as shown in Figure 5. The original $TM_{01}$ mode of the square patch is at about $f_0 = 4.8$ GHz and $(f_0 - f_2) > (f_1 - f_0)$. As a result, the uniformity of current distribution at $f_2$ is worse than that of at $f_1$, as shown in Figure 4; the direction of the radiation pattern at $f_2$ deviates from the broadside

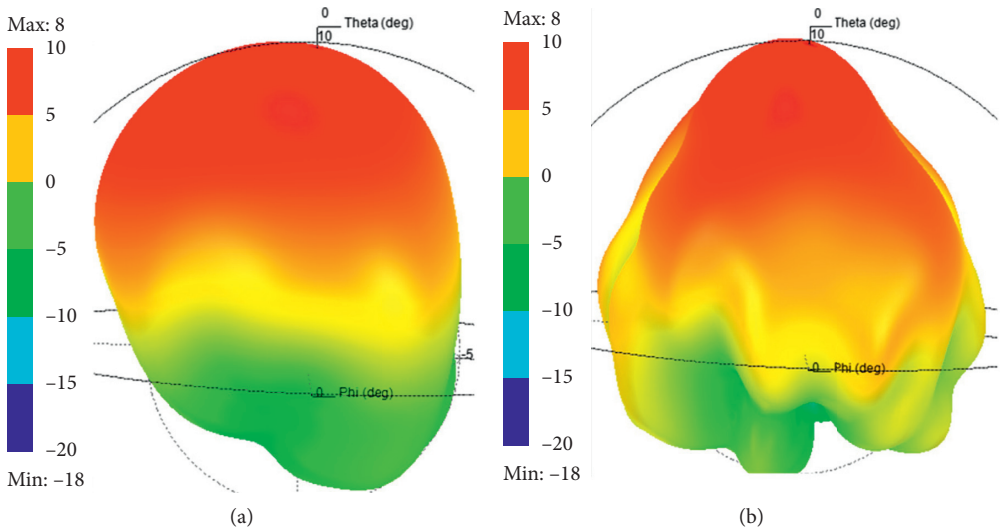


FIGURE 5: 3D radiation square patch of Design 1: (a) $f_2 = 3.75$ GHz and (b) $f_1 = 5.35$ GHz.

direction in some degree, but the $TM_{01}$ mode at $f_1$ still has a maximum of radiation in the broadside direction, as shown in Figure 5.

*3.2. Generation of Monopole-like Mode.* By utilizing a rectangular metal sheet, which is shorted to the ground plane by two conductive vias, a monopole-like ZOR mode for the square radiation patch is achieved, and that is the most outstanding contribution of the proposed design. Experimental results show that the performance of the ZOR mode is robust to the location change of the probe feed, and that is different from the reported omnidirectional antennas [16, 17], of which probe feeds must be fixed at the center of the circular radiation patch. In our design, there are the two clearance circles around the two conductive vias, which isolates the top-loaded rectangular metal sheet and the radiation square patch, so the probe feed can be located off-center without affecting the monopole-like radiation pattern.

For illustrating the excitation principle of the ZOR, an equivalent circuit of the proposed triband square patch antenna is derived and is shown in Figure 6. $L_f$ models the inductance of the feed probe, $L_P$ describes the inductive effect associated to the radial currents flowing on the square radiation patch, and $C_R$ is the capacitance of the annular slot. The capacitive coupling between the square patch part inside the annular slot and the ground plane is expressed by $C_{P1}$; $C_{P2}$ is the capacitive coupling between the part of the square patch outer the annular slot and the ground, while $C_M$ is the capacitive coupling between the rectangular metal sheet and the square radiation patch. The inductances of the conductive vias and the rectangular metal sheet are modeled by $L_v$ and $L_M$, respectively, while $R_P$ represents the antenna radiation resistance. By applying the rectangular metal sheet and the two conductive vias, two parallel branches both having $L_v$ and $L_M/2$ are introduced and can be replaced by one branch with an inductance of $(L_v + L_M/2)/2$. The branch having $C_M$ and $(L_v + L_M/2)/2$ is parallel to the branch with

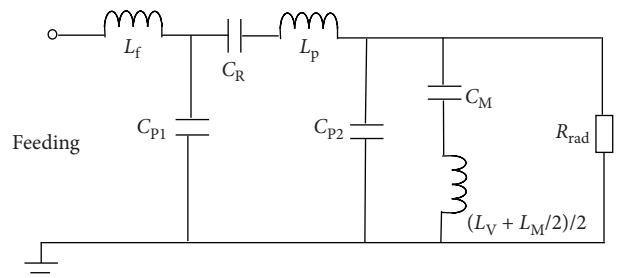


FIGURE 6: Equivalent circuit of the proposed triband patch antenna.

$C_{P2}$, ZOR mode is only related to the shunt components [18], and thus the proposed square patch antenna can support a ZOR mode at around 2.6 GHz.

The effects of the square patch side length $L_p$ and rectangular metal sheet width $M_w$ on the input impedance and $|S_{11}|$ of the proposed antenna are studied in Figures 7(a) and 7(b), respectively. For the lowest resonant mode at about 2.6 GHz, the resistance tends to the maximum value of about 50 Ω when the reactance of the input impedance goes to zero, which proves that the lowest resonant mode is a parallel resonant mode. In Figure 7(a), we also can see that the two $TM_{01}$ modes both are series resonant modes. The parallel resonant mode at about 2.6 GHz is also a ZOR mode, which is related to the shunt components; its resonant frequency is not affected by the varying $L_p$ in theory, since its resonant frequency depends on antenna reactance rather than antenna physical dimensions. However, a smaller $L_p$ brings to a smaller effective area of capacitor plate between the square patch and the ground plane and gives rise to a smaller capacitance $C_{P2}$. Then the resonant frequency of the ZOR mode moves to the higher frequency, but this tendency can be held up by increasing the value of $C_M$ and that can be deduced from Figure 6. A larger $M_w$ results in a larger $C_M$. When $L_P$ is decreased from 26 to 23 mm, $M_w$ is increased from 4.8 to 8.8 mm correspondingly; resonant frequency of

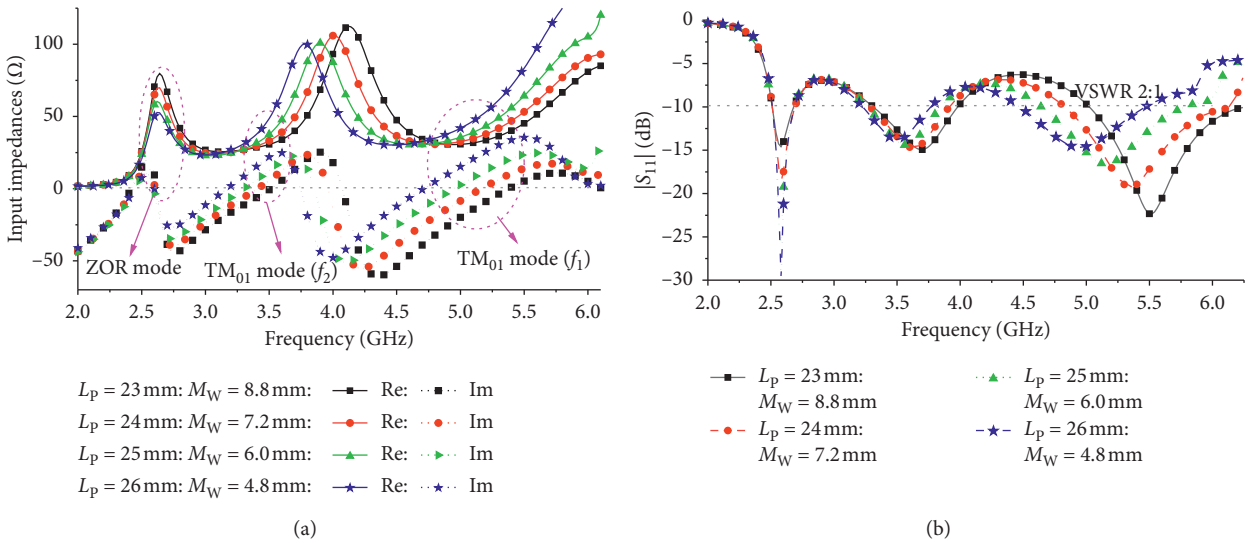


FIGURE 7: The effects of $L_P$ and $M_W$ on (a) input impedances and (b) $|S_{11}|$ of the proposed patch antenna.

the ZOR mode is preserved at around 2.6 GHz, as shown in Figures 7(a) and 7(b). However, despite the fact that a larger $M_w$ is chosen, the resonant frequencies of the two $TM_{01}$ modes move towards the higher frequencies with the decreasing of $L_P$, as shown in Figure 7.

Moreover, the increase of the rectangular metal sheet length $M_L$ also leads to an increase of $C_M$; the ZOR mode resonant frequency shifts to the lower frequency, as shown in Figure 8, but the two $TM_{01}$ modes are almost not affected by $M_L$. $L_M$ is decreased with the decrease in the distance $V_d$ between the two conductive vias, leading to a smaller antenna reactance, as shown in Figure 9(a). The resonant frequency of the ZOR mode, which mainly depends on the antenna reactance, moves to the lower frequencies, as shown in Figure 9(b). However, the effect of the varying $V_d$ on the resonant frequencies of the two $TM_{01}$ modes is slight. Observing from Figures 7–9, we can draw a conclusion that the resonant mode at about 2.6 GHz is ZOR mode and can be controlled by the dimensions of the top-load rectangular metal sheet, but it has ignorable effect on the dual-resonant $TM_{01}$ mode.

Figure 10 shows the variation of $|S_{11}|$ of the proposed antenna with respect to different $F_y$; its effects on the two $TM_{01}$ modes are the same as that shown in Figure 2, but for the ZOR mode, the effect can be neglected. In Figure 11, the 3D electric fields and the equivalent magnetic currents of the proposed triband square antenna are sketched for the cases of $F_y = 0$ mm and $F_y = 8.0$ mm. The electric field distributions for both the two cases are similar. Omitting the slight disturbances of the two conductive vias and the probe feed, the electric fields under the square patch and the rectangular metal sheet vary in phase and are uniformly vertical to the square patch for the two cases. Based on the cavity model of the patch antenna, the equivalent magnetic loop currents along square patch peripheries can be produced and give rise to perfect monopole-like radiation patterns, as presented in Figures 12(a) and 12(b). This is further proved that the performance of the ZOR mode is robust to the location change of the probe feed. The radiation patterns from the two $TM_{01}$ modes at 3.6 and 5.3 GHz are shown in Figures 12(b) and 12(c), and their performances are similar as that in Figures 5(a) and 5(b), respectively, showing once again that the effect of the rectangular metal sheet on the two $TM_{01}$ modes is very slight.

## 4. Results and Discussion

The proposed triband patch antenna with a profile of about $0.06\lambda_0$ at 2.5 GHz and dual-sense radiation patterns is fabricated, and its photographs are shown in Figure 13. The simulated and measured $|S_{11}|$ shown in Figure 14 are in a good agreement and both are less than −10 dB in 2.5–2.7 GHz, 3.3–3.9 GHz, and 4.8–6.1 GHz.

It is clear from Figure 15(a) that both the measured and simulated radiation patterns in *xy* and *xz* planes at 2.6 GHz show a monopole-like radiation pattern. The radiation patterns in *yz* and *xz* planes at 3.6 and 5.3 GHz are shown in Figures 15(b) and 15(c), respectively. It is observed that the antenna has the maximum radiation at the direction of Phi = 90° and Theta = −30° for 3.6 GHz, while the maximum radiation is in the broadside direction at 5.3 GHz, and that is because the uniformity of current distribution at $f_2$ is worse than that of at $f_1$, as shown in Figure 4. The simulated Co-pol pattern agrees well with the measured one, and the discrepancy for simulated and measured Cross-pol levels is due to the limit of the anechoic chamber. The results show that the proposed antenna has different radiation patterns for the three operation bands of 2.5–2.7 GHz, 3.3–3.9 GHz, and 4.8–6.1 GHz. Figure 16 shows the simulated and measured gains for the three operation bands are 2.0–3.2 dBi, 5.5–7.0 dBi, and 6.2–8.1 GHz, respectively. The measured efficiency is also given in Figure 16, and the efficiencies are higher than 77%, 84%, and 86% for the lower, middle, and highest operation bands, respectively.

Table 1 compares the proposed triband patch antenna with the other four reported antennas having omnidirectional and unidirectional radiation patterns. The comparison

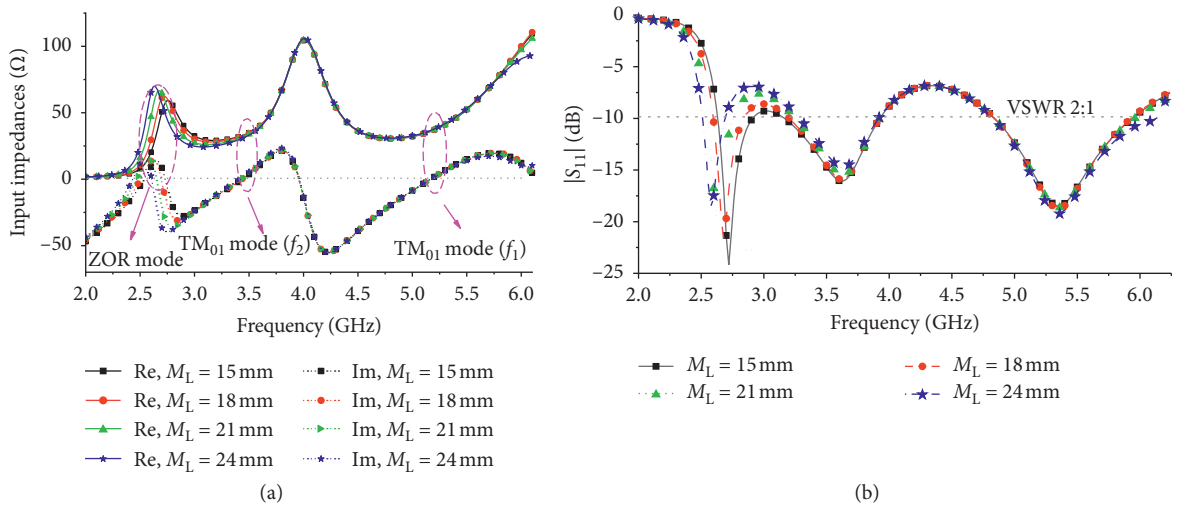


Figure 8: The effect of $M_L$ on (a) input impedances and (b)$|S_{11}|$ of the proposed patch antenna.

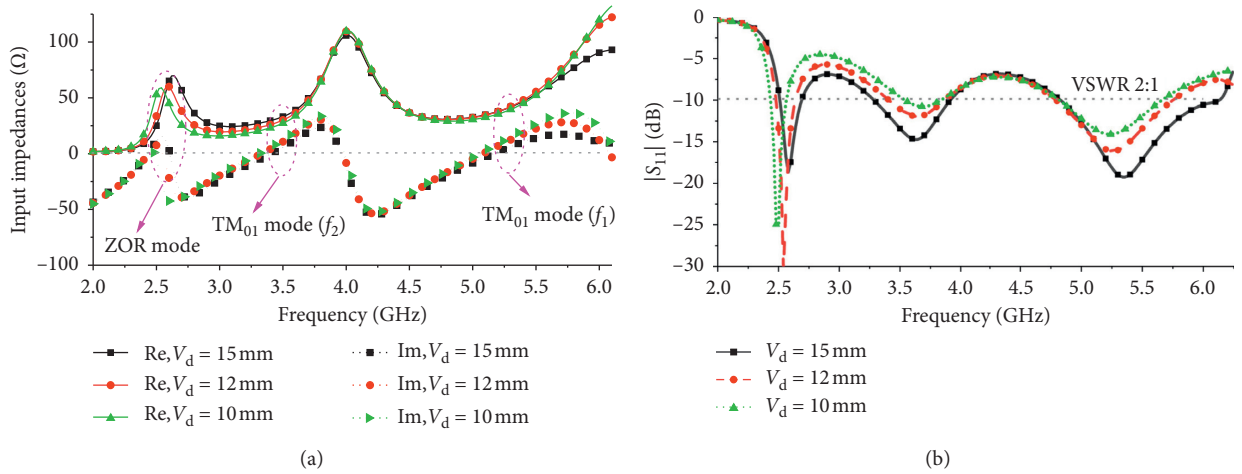


Figure 9: The effect of $V_d$ on (a) input impedances and (b) $|S_{11}|$ of the proposed patch antenna.

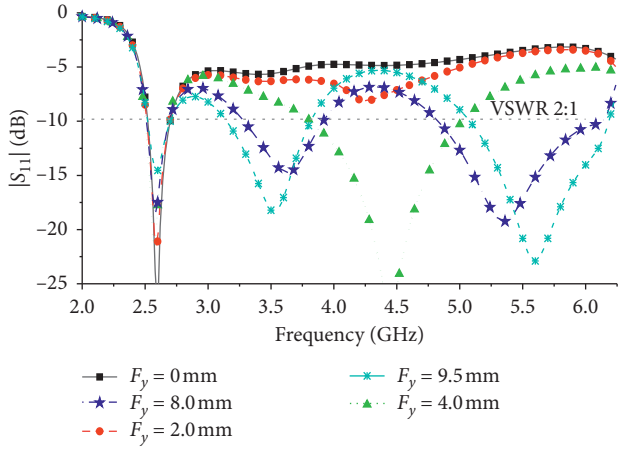


Figure 10: The effect of $F_y$ on $|S_{11}|$ of the proposed triband patch antenna.

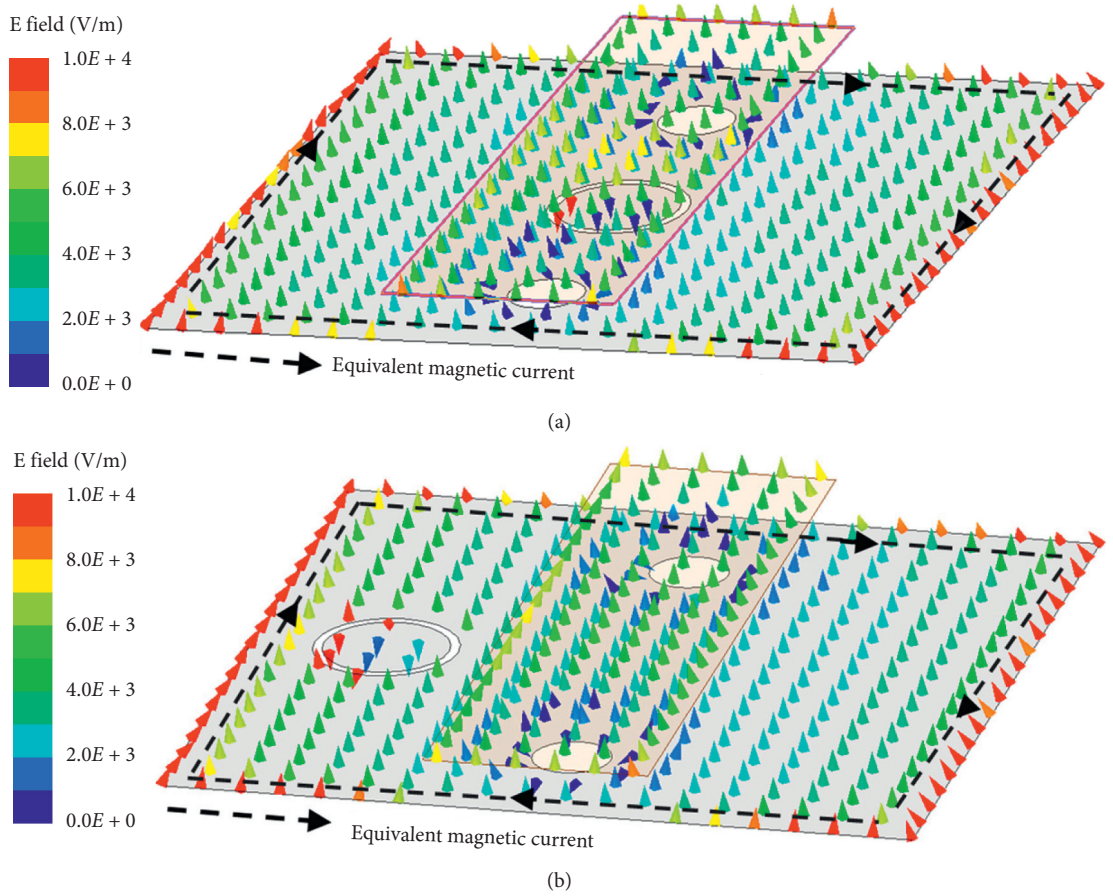


Figure 11: Distribution of electric field and equivalent magnetic current at 2.6 GHz of the proposed triband patch antenna: (a) $F_y = 0$ mm; (b) $F_y = 8.0$ mm.

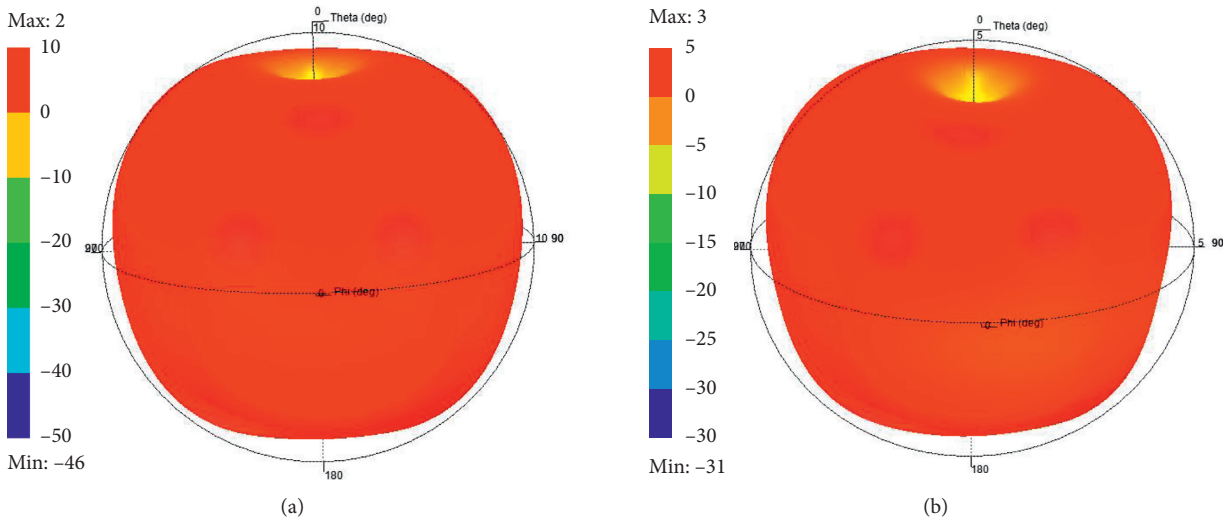


Figure 12: Continued.

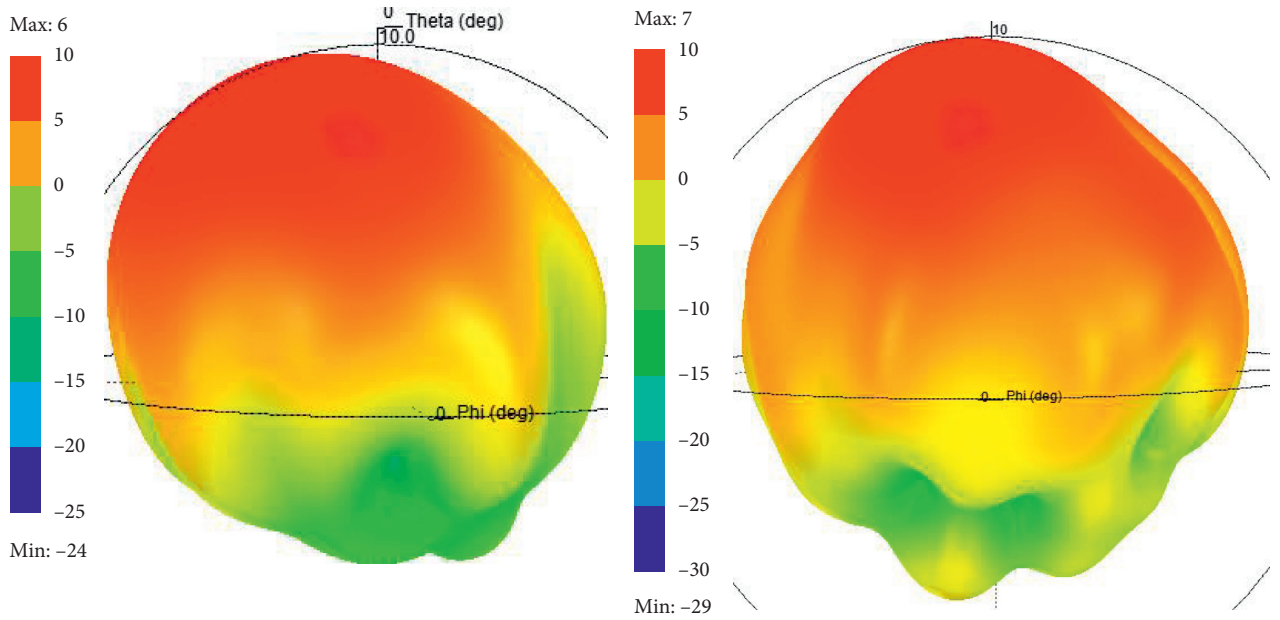


(c) (d)

Figure 12: 3D radiation patterns of the proposed antenna: (a) $f = 2.6$ GHz; $F_y = 0$ mm; (b) $f = 2.6$ GHz; $F_y = 8$ mm; (c) $f = 3.6$ GHz; $F_y = 8$ mm; (d) $f = 5.3$ GHz; $F_y = 8$ mm.

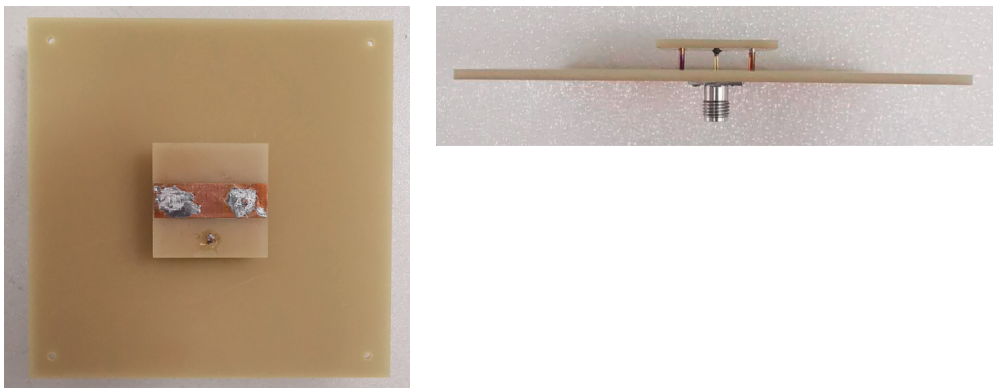

(a) (b)

Figure 13: Photograph of the fabricated antenna: (a) top and (b) size view.

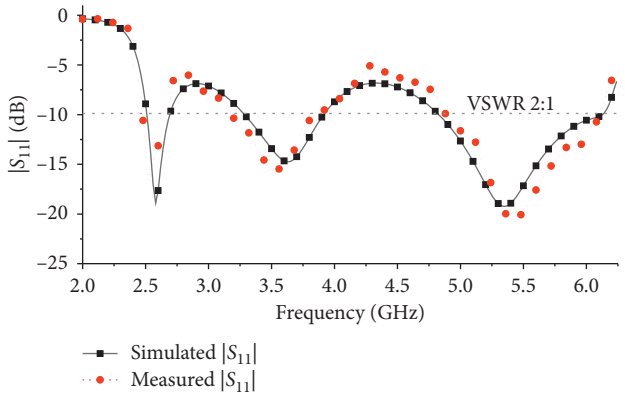


Figure 14: Simulated and measured $|S_{11}|$ of the proposed patch antenna.

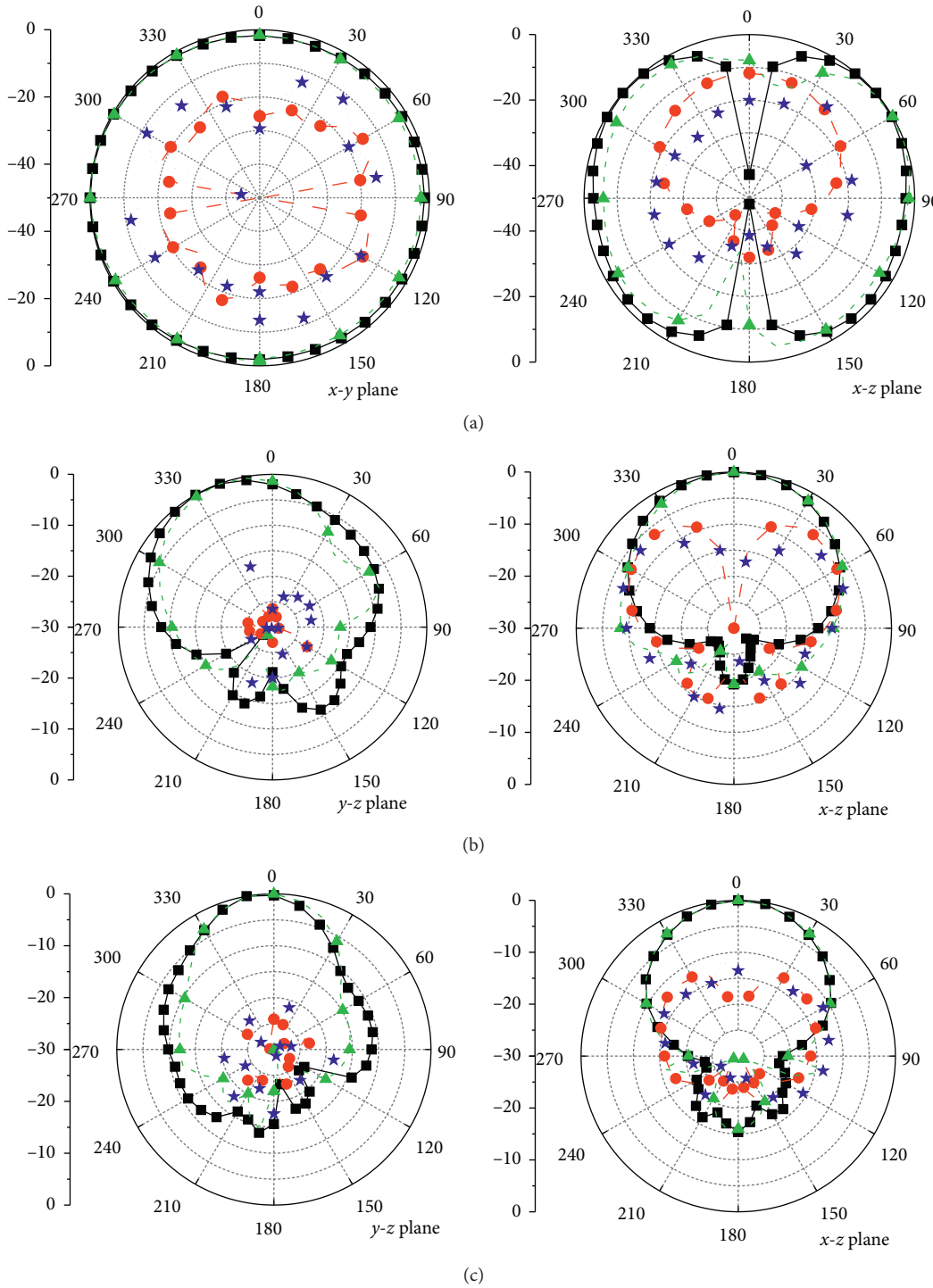


Figure 15: Simulated and measured radiation patterns of the proposed triband patch antenna at (a) 2.6 GHz, (b) 3.6 GHz, and (c) 5.3 GHz.

focuses on the number of antenna radiator, operation bands, size of antenna radiators in terms of their wavelengths at the lowest operating frequencies, antenna profiles in terms of wavelengths at the lowest operating frequencies, and the performance of radiation patterns. This comparison shows that just the proposed antenna, the antenna [14], and the antenna [19] employ a single one radiator to achieve the omnidirectional radiation pattern and the unidirectional radiation pattern simultaneously. However, the sizes of radiator for the two antennas [14, 19] are larger than that of the proposed antenna. The antenna [14] has a lower antenna profile compared with the proposed antenna, but only the proposed antenna has three operation bands. Comparing with the other antennas, we can say that the proposed antenna with a single square patch, compact size, low-profile, triband, monopole-like, and patch-like radiation

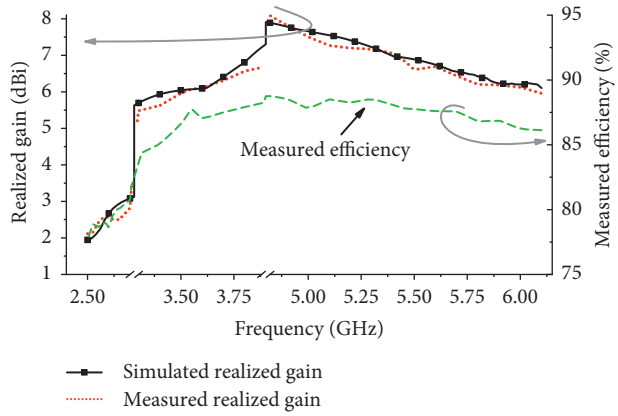


Figure 16: Realized gain and efficiency of the proposed patch antenna.

Table 1: Comparison with other antennas having omnidirectional and unidirectional radiation patterns.

| Antenna | Radiator number | Operation band | Size of radiator at the lowest operating frequencies | Antenna profile | Radiation pattern | | |
|---|---|---|---|---|---|---|---|
| | | | | | Lower band | Middle band | High band |
| [9] | 2 | Dual band | $0.026\lambda_0^2$ | $0.03\lambda_0$ | Omnidirectional | — | Unidirectional |
| [10] | 2 | Dual band | $0.694\lambda_0^2$ | $0.09\lambda_0$ | Unidirectional | — | Omnidirectional |
| [14] | 1 | Dual band | $0.0676\lambda_0^2$ | $0.26\lambda_0$ | Omnidirectional | — | Unidirectional |
| [19] | 1 | Dual band | $0.074\lambda_0^2$ | $0.047\lambda_0$ | Omnidirectional | — | Unidirectional |
| This work | 1 | Triband | $0.040\lambda_0^2$ | $0.06\lambda_0$ | Omnidirectional | Unidirectional | Unidirectional |

patterns is more suitable to be applied in the multifunctional communication system with limited space.

## 5. Conclusions

A compact triband antenna with a single square patch, low-profile, monopole-like, and patch-like radiation patterns has been presented. By using a rectangular metal sheet shorted to the ground plane, a small annular slot etched on the square radiation patch, and an off-center feed probe, a ZOR mode with monopole-like radiation pattern at the lowest operation has been obtained, and a dual-resonant $TM_{01}$ mode has been excited, yielding unidirectional radiation pattern for the middle and the highest operation bands. The triband antenna has been fabricated and tested, and the measured and simulated results are in a good agreement. The measured realized gain and the radiation efficiency in 2.5–2.7 GHz are 2.0–3.2 dBi and 77–80.5%, respectively. The measured realized gain and the radiation efficiency in 3.3–3.9 GHz are 5.5–6.8 dBi and 84–88%, respectively. The measured realized gain and the radiation efficiency are, respectively, 6.2–8.1 dBi and 86–88.5% in 4.8–6.1 GHz.

## Data Availability

The numerical and experimental data used to support the findings of this study are included within the article.

## Conflicts of Interest

The authors declare that there are no conflicts of interest regarding the publication of this paper.

## Acknowledgments

This work was supported by the National Science Foundation for Young Scientists of China under Grant 61901126. The authors would like to thank Professor Bin-Jie Hu for his invaluable assistance in the preparation of this manuscript.

## References

[1] Y. J. Guo, A. Paez, R. A. Sadeghzadeh, and S. K. Barton, "A circular patch antenna for radio LAN's," *IEEE Transactions on Antennas and Propagation*, vol. 45, no. 1, pp. 177-178, 1997.

[2] Y.-X. Guo, M. Y. W. Chia, Z. N. Chen, and K.-M. Luk, "Wide-band L-probe fed circular patch antenna for conical-pattern radiation," *IEEE Transactions on Antennas and Propagation*, vol. 52, no. 4, pp. 1115-1116, 2004.

[3] W. W. Wang, C. H. Chen, S. W. Wang, and W. Wu, "A wideband omnidirectional filtering patch antenna with high selectivity," *Microwave and Optical Technology Letters*, vol. 29, pp. 1–8, 2018.

[4] V. G. Posadas, D. S. Vargas, E. R. Iglesias, J. L. V. Roy, and C. M. Pascual, "Approximate analysis of short circuited ring patch antenna working at TM01 mode," *IEEE Transactions on Antennas and Propagation*, vol. 54, no. 6, pp. 1875–1879, 2006.

[5] A. Chapari, A. Zeidaabadi Nezhad, and Z. H. Firouzeh, "Analytical investigation of a low-profile multiband circular microstrip antenna with monopolelike radiation patterns," *IEEE Transactions on Antennas and Propagation*, vol. 66, no. 12, pp. 6810–6817, 2018.

[6] H. T. Huy, N. T. Nghia, and C. P. Hyun, "A compact wideband omnidirectional circularly polarized antenna using $TM_{01}$ mode with capacitive feeding," *IEEE Antennas and Wireless Propagation Letter*, vol. 18, no. 1, pp. 19–23, 2019.

[7] Y. M. Pan, S. Y. Zheng, and B. J. Hu, "Wideband and low-profile omnidirectional circularly polarized patch antenna," *IEEE Transactions on Antennas and Propagation*, vol. 62, no. 8, pp. 4347–4351, 2014.

[8] S. Gao, L. Ge, D. Zhang, and W. Qin, "Low-profile dual-band stacked microstrip monopolar patch antenna for WLAN and car-to-car communications," *IEEE Access*, vol. 6, pp. 69575–69581, 2018.

[9] J. D. Lin, Z. P. Qian, W. Q. Cao, S. J. Shi, Q. Q. Wang, and W. Zhong, "A low-profile dual-band dual-mode and dual-polarized antenna based on AMC," *IEEE Antennas and Wireless Propagation Letter*, vol. 16, pp. 2473–2476, 2016.

[10] L. Ge, S. Gao, Y. Li, W. Qin, and J. Wang, "A low-profile dual-band antenna with different polarization and radiation properties over two bands for vehicular communications," *IEEE Transactions on Vehicular Technology*, vol. 68, no. 1, pp. 1004–1008, 2019.

[11] H. Wong, K. K. So, and X. Gao, "Bandwidth enhancement of a monopolar patch antenna with V-shaped slot for car-to-car and WLAN communications," *IEEE Transactions on Vehicular Technology*, vol. 65, no. 3, pp. 1130–1136, 2016.

[12] S.-J. Lin and J.-S. Row, "Monopolar patch antenna with dual-band and wideband operations," *IEEE Transactions on Antennas and Propagation*, vol. 56, no. 3, pp. 900–903, 2008.

[13] Y. F. Cao, X. Y. Zhang, and T. Mo, "Low-profile conical-pattern slot antenna with wideband performance using artificial magnetic conductors," *IEEE Transactions on Antennas and Propagation*, vol. 12, no. 2, pp. 2210–2218, 2018.

[14] M.-S. Wang, X.-Q. Zhu, Y.-X. Guo, and W. Wu, "Compact dual-band circularly polarised antenna with omnidirectional and unidirectional properties," *IET Microwaves, Antennas & Propagation*, vol. 12, no. 2, pp. 259–264, 2018.

[15] A. Sanada, M. Kimura, L. Awai, C. Caloz, and T. Itoh, "A planar zeroth-order resonator antenna using a left-handed transmission line," in *Proceedings of the 34th European Microwave Conference*, vol. 3, pp. 1341–1344, Amsterdam, Netherlands, October 2004.

[16] S. Yan and G. A. E. Vandenbosch, "Zeroth-order resonant circular patch antenna based on periodic structures," *IET Microwaves, Antennas & Propagation*, vol. 8, no. 15, pp. 1432–1439, 2014.

[17] Y. Guo, J. Zhao, Q. W. Hou, and X. P. Zhao, "Omnidirectional broadband patch antenna with horizontal gain enhanced by epsilon-negative metamaterial superstrate," *Microwave and Optical Technology Letters*, Early View, Hoboken, NJ, USA, 2019.

[18] S.-T. Ko and J.-H. Lee, "Hybrid zeroth-order resonance patch antenna with broad $E$-Plane beamwidth," *IEEE Transactions on Antennas and Propagation*, vol. 61, no. 1, pp. 19–25, 2013.

[19] D.-L. Wu, G. Zhang, J.-F. Li, Y.-J. Wu, and X.-X. Tian, "A low-profile antenna with omnidirectional and unidirectional radiation patterns over two operation bands," *IEEE Access*, vol. 7, pp. 182691–182700, 2019.

[20] D. M. Pozar, *Microwave Engineering*, Wiley, New York, NY, USA, 2nd edition, 1998.

[21] K. F. Lee, K. Ho, and J. Dahele, "Circular-disk microstrip antenna with an air gap," *IEEE Transactions on Antennas and Propagation*, vol. AP-32, pp. 880–884, 1987.

[22] K. Carver and J. Mink, "Microstrip antenna technology," *IEEE Transactions on Antennas and Propagation*, vol. 29, no. 1, pp. 2–24, 1981.